Engineering in Life Sciences

Specific ion effects on the particle size distributions of cell culture-derived influenza A virus particles within the Hofmeister series

Journal:	*Engineering in Life Sciences*
Manuscript ID	Draft
Wiley - Manuscript type:	Research Article
Date Submitted by the Author:	n/a
Complete List of Authors:	Pieler, Michael; Max Planck Institute for Dynamics of Complex Technical Systems, Bioprocess Engineering (BPT) Schenk, Anja; Otto von Guericke Universitat Magdeburg Wolff, Michael; Max Planck Institute for Dynamics of Complex Technical Systems, Bioprocess Engineering (BPT); Otto von Guericke Universitat Magdeburg Reichl, Udo; Max Planck Institute for Dynamics of Complex Technical Systems, Bioprocess Engineering (BPT); Otto von Guericke Universitat Magdeburg
Keywords:	Hofmeister series, specific ion effects, vaccines, viral vectors, virus aggregation

Research Article

Specific ion effects on the particle size distributions of cell culture-derived influenza A virus particles within the Hofmeister series

Michael Martin Pieler[1]

Anja Schenk[2]

Michael Werner Wolff[1,2]

Udo Reichl[1,2]

[1] Max Planck Institute for Dynamics of Complex Technical Systems, Sandtorstr. 1, 39106 Magdeburg, Germany

[2] Otto von Guericke University Magdeburg, Universitätsplatz 2, 39106 Magdeburg,

Correspondence: Michael M. Pieler (pieler@mpi-magdeburg@mpg.de). Bioprocess Engineering, Max Planck Institute for Dynamics of Complex Technical Systems, Sandtorstr. 1, 39106 Magdeburg, Germany

Keywords: Hofmeister series; specific ion effects; vaccines; viral vectors; virus aggregation

Abbreviations: **A/PR**, A/Puerto Rico/8/1934; **AHD**, apparent hydrodynamic diameter maxima; **AUC**, analytical ultracentrifugation; **CCC**, critical coagulation concentration; **CFV**, concentrated and filtered virus samples; **CSC**, critical stabilization concentration; **CVH**, clarified virus harvests; **DCS**, differential centrifugal sedimentation; **DSP**, downstream processing; **EM**, electron microscopy; **FCS**, fetal calf serum; **GB**, gradient buffer; **HA**, hemagglutinin; **HAU**, HA units; **HS**, Hofmeister series; **MDCK**, Madin Darby canine kidney; **MOI**, multiplicity of infection; **MWCO**, molecular weight cut-off; **NA**, neuraminidase; **PBS**, phosphate buffer saline; **PMMA**, poly(methyl methacrylate); **PSD**, particle size distribution;

PVC, polyvinyl chloride; **RPM**, revolutions per minute; **RT**, room temperature; **SB**, standard buffer; **SPA**, single particle approximation; **VP**, Virus particle.

Practical application

This work shows the practical application of a differential centrifugal sedimentation (DCS) disc centrifugation method for virus particle size distribution screenings (PSDs). The high resolution and accuracy of the implemented PSD measurement method offered interesting insights on the (aggregation) behavior of influenza A/Puerto Rico/8/34 (H1N1) virus particles in different buffer systems. Therefore, the method's applicability for screening of other biological colloidal particle systems, like vaccine or viral vector formulations, is feasible. Considering the large impact of virus particle size and aggregation behavior on downstream processing yields as well as formulation and blending of vaccines and gene therapy vectors our results address important issues concerning process optimization and product quality.

Abstract

Virus particle (VP) aggregation can have serious implications for clinical safety and efficacy of virus-based therapeutic products. Typically, VPs are suspended in buffers to establish defined product properties. Salts used to achieve these properties show specific effects in chemical and biological systems in a reoccurring trend known as Hofmeister series (HS). HS effects are ubiquitous and can affect colloidal particle systems. In this study, influences of different ions (anions: SO_4^{2-}, HPO_4^{2-}, Cl^-, Br^-, NO_3^-, I^-; cations: K^+, Na^+, Li^+, Mg^{2+}, Ca^{2+}) on particle size distributions (PSDs) of cell culture-derived influenza VPs were investigated. For the experimental setup, influenza virus A/Puerto Rico/8/34 (H1N1) produced in Madin Darby canine kidney (MDCK) cells was used. Inactivated and concentrated virus harvests were dialyzed against buffers containing ions of interest, followed by analysis via differential centrifugal sedimentation to measure PSDs. VPs from both cell lines showed no aggregation over a wide range of buffers containing different salts in concentrations ≥ 60 mM. However, VPs produced in adherent cells showed increased aggregation compared to VPs produced in suspension cells when dialyzed to low salt or Ca^{2+} buffers. Additionally, changes in VP diameters depending on specific ion concentrations were observed that partially reflected the HS trend.

1 Introduction

Virus particle (VP) aggregation is an important factor to be considered for the optimization of the production of viral vaccines, i.e., VP quantification, in vitro infectivity assays [1], inactivation of VP [2–4], and downstream processing (DSP) [5]. Accordingly, the characterization of media and buffer components affecting the virus particle size distribution (PSD) is of great interest. Previous investigations used complex methods to analyze virus PSDs. For example, pioneering work in this field used a "single particle approximation" (SPA) method employing high-speed centrifugation for separating monomeric VPs from multimers to investigate VP aggregation by diluting polio- and reoviruses in water [6,7], the survival of such aggregates [2], the effects of certain salts on VP aggregation at low pH [8], and the occurrence of mixed aggregates of both VP species [9]. The VP separation via SPA was achieved by stopping centrifugation at a certain time point followed by analysis of the different layers of the centrifuged sucrose gradient fluid by plaque titration or electron microscopy (EM). Furthermore, influenza VP aggregation has been investigated with a modified SPA method in combination with EM to determine the VP content of influenza vaccines [10]. Results showed that all analyzed vaccines contained to some degree VP aggregates, which could be dispersed by suspension in high molality buffers. More recent experimental studies explored the effects of certain hemagglutinin (HA) and neuraminidase (NA) gene combinations on the aggregation status of influenza VPs by centrifugation in a sucrose gradient followed by analyzing the different layers of the centrifuged fluid by a HA assay [11]. Furthermore, pH-induced aggregation of influenza VPs was studied by static and dynamic light scattering [12], and UV absorption [13]. Unfortunately, none of these methods gives detailed PSDs of the VPs and their aggregates, which are needed to better understand the involved effects.

An established method to obtain high-resolution size distributions of colloids is analytical ultracentrifugation (AUC) [14]. High-end AUC equipment involves substantial costs for equipment and operation and therefore makes it only suitable for specialized research taking full advantage of its features. Since several years, however, comparatively simple centrifuges for

particle size analysis are available that use limited rotor speeds and fixed single wavelength detection systems [14]. One example is the CPS DC24000 UHR disc centrifuge from CPS Instruments Inc. (LA, USA) employing differential centrifugal sedimentation (DCS) [15]. The implemented DCS method determines the sedimentation times of the particles of interest with unknown size but known buoyant density in a gradient fluid with known density to calculate their sizes based on Stokes' law [15]. Applications reported so far included the characterization of PSDs of recombinant adeno VP [16,17], L1 virus-like particles [18], and influenza VPs [19]. Finally, the use of a DCS method enables the determination of PSDs with a higher resolution than other dynamic light scattering techniques [20].

The experimental setup for determining PSDs of influenza VPs in the present work is based on a DCS disc centrifugation method to investigate specific ion effects within the HS on influenza virus PSDs. The order of the direct HS is $SO_4^{2-} < HPO_4^{2-} < Cl^- < Br^- < NO_3^- < I^-$ for the anions, and $K^+ < Na^+ < Li^+ < Mg^{2+} < Ca^{2+}$ for the cations and the indirect HS has the reverse order [21–23]. The ions are ordered according to their effect on the solubility of proteins: Early members of the direct HS series increase the solvent surface tension and decrease the solubility of nonpolar molecules ("salting out", kosmotropic) while the later salts increase the solubility of nonpolar molecules ("salting in", chaotropic) [23,24]. In addition, HS effects on synthetic nanoparticles were described in literature [23,25–30]. For biological nanoparticles like VPs, however, no systematic evaluations of HS effects by high resolution PSD measurement techniques have been carried out so far. Therefore, the present work delivers fundamental information regarding the effects of certain HS ions on the PSDs of cell culture-derived influenza VPs by DCS disc centrifugation.

2 Materials and Methods

2.1 Buffer and media solution preparation

Ultrapure water from a Milli-Q® Advantage A10 water purification system from Merck KGaA (Darmstadt, Germany) was used for all buffers and media solutions. All chemicals used for HS

buffers had a purity of ≥99% and were obtained from Sigma-Aldrich Co. LLC. (St. Louis, USA) unless otherwise stated; all chemicals used for cell culture media were cell culture media grade. The salts for the HS buffers used for screening were Na_2SO_4 (#S9627), Na_2HPO_4 (#S8282), NaH_2PO_4 (#S7907), NaCl (#S7653), NaBr (#71329), $NaNO_3$ (#S8170), and NaI (#793558) for the anions, and $CaCl_2$ (#C5080), KCl (#P9333), LiCl (#62476), and $MgCl_2$ (#M2670) for the cations. Na^+ or Cl^- salts were used as they are considered reference points in the HS [26]. The concentrations used for the screening were 20, 60, 540 mM for all HS salts, and for NaCl additionally 180, 1020, and 1500 mM. All HS ion concentrations in the HS buffers were based on the specific ion of interest without adjusting the HS buffer recipe for the counterions. For the preparation of all HS buffers a minimal 10 mM Tris-HCl standard buffer (SB) system was used to maintain the pH at 7.4. All HS buffers were prepared and used at room temperature (RT, 25°C) to avoid pH shifts due to the high temperature dependency of the Tris pKa [31]. For the preparation of 500 ml HS buffer, 0.605 g Tris base (#T6791) and the amount of the HS salt of interest were dissolved in approximately 450 ml ultrapure water, followed by subsequent titration to pH 7.4 with HCl (#100317, Merck KGaA, Darmstadt, Germany) diluted in ultrapure water and filled up to 500 ml with ultrapure water. For the Na^+/PO_4^{3-} buffer, the acidic and basic compounds (NaH_2PO_4 and Na_2HPO_4) were weighted to result in pH 7.4 followed by titration with HCl after addition of Tris-base and ultrapure water. Additionally, NaN_3 (#71290) was added to a final concentration of 0.05% to the HS buffers to inhibit microbial growth, and filtered with a 0.2 µm bottle top filter (#514-0340, VWR, Radnor, USA) to remove particulate impurities. HS buffers were stored at 4°C and were allowed to warm-up to RT before usage.

2.2 Haemagglutination assay for virus quantification

The haemagglutination (HA) assay was based on Kalbfuss et al. [32] The obtained HA units (HAU) from the HA assay correlate to the number of VPs in the sample.

2.3 Influenza virus particle production

Influenza VPs were produced in a suspension ($MDCK_{SUS2}$) and an adherent Madin Darby canine kidney (MDCK) cell line ($MDCK_{ADH}$, ECACC No. 84121903) by infection with an in-house generated adherent MDCK-derived A/Puerto Rico/8/34 (A/PR, H1N1) virus seed (#3138, Robert Koch Institute, Berlin, Germany) with a 50% tissue culture Infective Dose ($TCID_{50}$) of $1.23x10^8$ infectious VPs/mL [33–35].

$MDCK_{SUS2}$ cells were cultivated in chemically defined, protein- and peptide-free SMIF8 PGd medium (used 2x concentrated, #M008-2b, Service Zellkultur Scharfenberg, Emden, Germany). Additionally, this medium contained 4 mM L-glutamine, 4 mM pyruvate, 5 g/L NaCl, 3.66 g/L D-(+)-glucose, 2 g/L NaHCO3, 0.242 g/L L-glutamic acid, 10 mL/L 10% Pluronic-F68, and 1 µL/L 98% ethanolamine. For virus infection, 10^{-5} trypsin units/cell (#27250-018, from porcine pancreas, Thermo Fisher Scientific, Massachusetts, USA) was added. Cultivations were carried out in a 5 L CT5-SK bioreactor from Sartorius Stedim Biotech GmbH (Göttingen, Germany). For virus production, a multiplicity of infection (MOI) of 10^{-4} was used, and the virus broth was harvested 72 hours post infection (hpi). VPs produced by $MDCK_{SUS2}$ are subsequently termed as "A/PR_{SUS}".

$MDCK_{ADH}$ cells were cultivated in GMEM-BHK21 medium (#22100-093, Thermo Fisher Scientific, Massachusetts, USA). Additionally, the medium was supplemented with 1 g/L D-(+)-glucose, 4 g/L $NaHCO_3$, 10% fetal calf serum (FCS, #F7524, Sigma-Aldrich Co. LLC., St. Louis, USA), 2% lab-FMV-peptone (#MC033, Lab M Ltd., Heywood, UK). For virus production, cells were washed three times with 1x phosphate buffer saline (1x PBS) and fresh medium without FCS and with $5x10^5$ trypsin units/mL was added. The VP production was carried out in 850 cm^2 roller bottles (#680160, Greiner Bio One International GmbH, Frickenhausen, Germany) with 0.5 ml of the in-house generated A/PR virus stock using a MOI of 10^{-4}. The virus broth was harvested 72 hpi. VPs produced by the $MDCK_{ADH}$ system are subsequently termed as "A/PR_{ADH}".

2.4 Virus broth clarification and inactivation

Harvested virus broths were filtered through a 5 µm depth filter followed by a 0.65 µm depth filter (#CFAP0508YY and #CFAP9608YY, GE Water & Process Technologies, Trevose, USA). After clarification, chemical inactivation with β-propiolactone (#33672.01, Serva Electrophoresis, Heidelberg, Germany) at a final concentration of 6 mM was carried out. The inactivation process was stopped after incubation at 37°C for 24 h and completed by a filtration through a 0.45 µm depth filter (#CMMP9408YY, GE Water & Process Technologies, Trevose, USA) to obtain clarified virus harvests (CVH).

2.5 Concentration of the clarified virus harvest by tangential flow filtration

For concentrating both CVHs to approximately 10^5 HAU/mL a Sartocon Slice 200 Hydrosart tangential flow filtration (TFF) cassette (cellulose membrane) kindly provided by Sartorius Stedim Biotech GmbH (Göttingen, Germany) with a molecular weight cut-off (MWCO) of 750 kDa, was used. The concentration via TFF was carried out on an Äkta crossflow TFF system from GE Healthcare Bio-Sciences AB (Uppsala, Sweden). After concentration, both CVHs were filtered through a 0.1 µm filter (#SLVV033RS, Merck KGaA, Darmstadt, Germany), aliquoted, and frozen at -80°C to obtain concentrated and filtered virus samples (CFV). The final filtration step ensured that VP aggregates are only newly formed form monomeric VPs in the course of the subsequent experiments.

The A/PR_{SUS} CVH was 10x concentrated by volume reduction to obtain the A/PR_{SUS} CFV with $9.6x10^4$ HAU/mL after 0.1 µm filtration, aliquotation, freezing (-80°C) and thawing. Using the same approach A/PR_{ADH} CVH was 40x concentrated to A/PRADH CFV with $1.3x10^5$ HAU/mL. Because of the small difference in the concentrations, the higher concentrated A/PRADH CFV sample was diluted 1:1.4 in 1x PBS before the subsequent dialysis step (see next section) to a concentration of 10^5 HAU/mL. No VP aggregation was observed during the described sample preparation (data not shown).

2.6 Buffer exchange via dialysis

Dialysis was used to change the buffer of the CFV samples from cell culture media to the HS buffer of interest. Therefore, 500 µl CFV sample was pipetted into a cellulose dialysis tube with a MWCO of 14 kDa (#0653.1, Carl Roth GmbH & Co. KG, Kalrsruhe, Germany), and dialyzed against 500 ml HS buffer with a dialysis factor of $1:10^3$ under stirring for 24 h at RT. A 14 kDa MWCO dialysis membrane was used to avoid any potential impact of sample concentration during the buffer exchange step. In particular, dialysis membranes with higher cut-offs could induce aggregation because of volume reduction due to high osmotic pressures of higher concentrated HS buffers (data not shown).

2.7 Particle size distribution measurements by differential centrifugal sedimentation

A DCS method was used for measuring PSDs of the dialyzed CFV samples [15]. The used method was based on Neumann et al. [19], with additional modifications of the setup as described below.

A CPS DC24000 UHR disc centrifuge (CPS Instruments Inc., LA, USA) was used for measuring the virus PSDs at a maximum disc speed of 24.000 revolutions per minute (RPM). The gradient buffer (GB, 4 to 16% (w/v)) was prepared in the respective HS buffer using sucrose (#1.07654, Merck KGaA, Darmstadt, Germany). Therefore, 16%, 14.5%, 13%, 11.5%, 10%, 8.5%, 7%, 5.5%, and 4% (w/v) 1.6 ml GB steps with a total GB volume of 14.4 ml were injected. To reduce the risk of conformational changes of proteins adsorbed to dodecane-in-water emulsion interfaces no dodecane cap was added to prevent GB evaporation [36,37]. After building up the GB, 100 µl of a 239 nm particle standard (0.3 - 0.5% solid content, polyvinyl chloride (PVC), particle density $\rho_P = 1.385$ g/cm^3, CPS Instruments Inc., LA, USA) diluted 1:4.25 in HS buffer was injected to assess gradient quality. (Note: Injection of this particle standard not only ensured GB functionality, but also increases gradient life time by reducing evaporation at the gradient top surface.) Next, the gradient was equilibrated 10 min followed by another injection of the 239 nm particle standard for calibration (100 µl diluted 1:4.25 in HS buffer). Then, 100 µl of the dialyzed CFV sample was injected for the measurement. After each

measurement, the centrifuge disc was cleaned on the in- and outside with warm water to remove any residual gradient solution, and finally wiped out with pure isopropanol.

2.8 Gradient buffer and virus particle density measurements by differential centrifugal sedimentation

To determine the analysis parameters for the proprietary software of the CPS DC24000 UHR disc centrifuge, a density measurement method for deriving the GB density ρ_{GB} and the VP buoyant density ρ_{VP}, or – in general – the particle buoyant density ρ_P, was used [19]. Thus, for determining ρ_{GB} and ρ_{VP} of the sample, 100 µl of the VP sample was spiked with a 105 nm particle standard (final dilution of 1:8 in 100 µl sample, 5% (w/w) solid content, poly(methyl methacrylate) (PMMA), particle density ρ_P = 1.19 g/cm^3, #PMMA-R-KM215, Microparticles GmbH, Berlin, Germany), and a 239 nm particle standard (final dilution of 1:16 in 100 µl sample, 0.3 - 0.5% (w/w) solid content, PVC, particle density ρ_P = 1.385 g/cm^3, CPS Instruments Inc., LA, USA). The spiked samples were measured in triplicate in a 4 to 16% (w/v) and an 8 to 20% (w/v) sucrose GB.

The ρ_{GB} can be determined by linear regression from the measured sedimentation time t_{Std}, the known densities ρ_{Std}, and the hydrodynamic diameters D_{Std} of the standard particles (see equation 1-3 in the supporting information). (Note: ρ_{GB} can also be determined by measuring the weight of a defined volume of GB according to the setup of Neumann et al. [19] However, measuring ρ_{GB} in the DCS setup itself using the applied method will lead to more accurate values. With this setup the fluid of the standard particle injection on top of the GB, the GB evaporation over time, and the slightly different GB viscosities inside the warmed-up centrifuge disc are influencing the ρ_{GB} determination. Additionally, the GB below the detector beam is not contributing to the determined sedimentation times and therefore to the "effective" ρ_{GB}, and thus does not need to be taken into account at al. [38])

For determination of the ρ_{VP}, the GB density of the 4 to 16% (w/v) ($\rho_{GB4\text{-}16\%}$) and the 8 to 20% (w/v) ($\rho_{GB8\text{-}20\%}$) sucrose GB are determined by linear regression from the sedimentation times of

the standard particles $t_{Std105nm}$ and $t_{Std239nm}$ (see equation 4-6 in the supporting information). Then, the ρ_{VP} can be derived from the sedimentation times of the standard particle $t_{Std105nm}$ and the VP t_{VP} by an additional linear regression. For the determination of ρ_{VP}, the 105 nm particle standard was used as it is closer to VP size and buoyant density. The ρ_{VP} was determined for A/PR_{SUS} and A/PR_{ADH} VP in GB buffers made of 1x PBS. (Note: Linear regression analysis was based on previous work from A. Neumann et al. [19] and is explained in detail in the supporting information.)

3 Results and Discussion

To measure the specific ion effects of the HS buffers on the virus PSDs, a two stage experimental setup was carried out. First, the VP buoyant densities ρ_{VP} for the two samples were determined. In a next step the prepared VP samples were dialyzed and their PSDs were analyzed.

3.1 Virus particle density measurements by differential centrifugal sedimentation

The VP buoyant density ρ_{VP} determined by regression analysis of the sedimentation times in two different GBs were 1.17 g/cm^3 for the A/PR_{SUS} VP and 1.18 g/cm^3 for the A/PR_{ADH} VP, respectively (data not shown). Both values are similar to reported values for MDCK cell culture-derived influenza A virus strains, i.e., 1.18 and 1.19 g/cm^3 measured by the same method [19]. An example for the determination of time differences for sedimentation in two different GB (4-16% and 8-20% sucrose) is shown in Figure 1A for A/PR_{ADH} VP spiked with the 105 and 239 nm particle standard.

3.2 Specific ion effects on the particle size distributions of the virus particles

The screened HS buffers for influenza A/PR_{SUS} VPs were standard buffer (SB, 10 mM Tris-HCl pH 7.4), SB including 20, 60, and 540 mM of all HS ions as well as SB with 180, 1020, and 1500 mM for NaCl. Influenza A/PR_{ADH} VPs were screened in SB, SB with 20 mM NaCl as well

as SB with 20, 60 and 540 mM Ca^{2+}. The HS ion screening for concentrations higher than 540 mM was not possible for all buffers as density differences between VPs and GBs were not sufficient for the measurements (data not shown). In the following section the apparent hydrodynamic diameter maxima (AHD) of the monomeric or multimeric VPs (n = 3) is reported.

The virus PSDs for A/PR_{SUS} in SB with different concentrations of NaCl are shown in Figure 1B. Overall, AHDs increased with higher NaCl concentrations ($p < 0.05$, two-sample F-test and T-test between neighboring AHDs), except for 540 and 1020 mM ($p > 0.05$, details shown in Supplement Table 1). Regarding the aggregation behavior, all VPs in GBs with NaCl showed just a minor dimer peak between 100 to 110 nm. Only the size distribution obtained in SB was different showing high levels of dimers, trimers and even tetramers. For the measured multimer pattern the predicted AHDs of the aggregates ($D_{app,i}$, i = number of particles in the aggregate) based on deformable spheres agree well to theoretical values: maxima monomeric VP (D_{VP}) = 81 nm; dimer = 101 nm ($D_{VP:Dapp,2}$ = 1:1.25); trimer = 115 nm ($D_{VP:Dapp,3}$ = 1:1.42) [39]. The suitability of the prediction based on deformable spheres can be explained by the deformability of influenza A VPs shown in previous AUC studies [40]. However, for other measurements carried out in this study, the agreement between the measured and the theoretical AHD was sometimes better approximated by a rigid sphere model or both models, i.e., deformable and rigid spheres, failed to describe the measured AHDs (data not shown). Comparable VP aggregation in low salt buffers and water were reported before for influenza A/B, polio-, and reovirus by EM where large aggregates consisting of hundreds of VPs were found [7,10]. However, the latter is most likely not due to differences in buffers but an artifact due to sample preparation in EM. For the experimental setup and the analytical method used in our study, the formation of such large aggregates is not to be expected.

Particle aggregation is often described by a so-called critical coagulation concentration (CCC) and a critical stabilization concentration (CSC) [23,25–27]. These two concentrations are separating slow or reaction controlled regimes from fast or diffusion controlled regimes [23,26].

Furthermore, it is known that aggregation of weakly charged particles is fast in high salt concentrations and highly charged particles aggregate slowly in high salt concentrations [23]. Additionally, the CCC decreases with increasing counterion valence, which is known as Schulze-Hardy rule [23]. Taken together, it has to be expected that the investigated A/PR_{SUS} VP are highly charged and have a CSC below 20 mM NaCl. Moreover, such low CSC values indicate a high hydrophilicity of the investigated VP [26].

Remarkably, all measured size distributions with visible aggregates still showed a monomeric VP peak which indicates incomplete aggregation to multimers. One explanation for that could be a very slow aggregation process, as PSDs were measured only after 24 h incubation. Additionally, one could argue that this is due to the chosen sucrose gradient employed in the measurement setup. Nevertheless, a sucrose gradient was also used in the study of R. C. Dunlap et al. who used a SPA method [10], and for the characterization of adenovirus in the study of S.-J. Shih et al. by a DCS disc centrifugation method, respectively [17]. In the latter, an 8 to 24% sucrose gradient was used and compared to a conventional AUC method without sucrose gradient and only showed consistent minor reductions on the detected aggregate levels [17]. This suggests that the addition of sucrose is not affecting the measured PSDs via DCS disc centrifugation.

Results of the monomeric AHDs for A/PR_{SUS} VPs are shown in Figure 2 for 20, 60, and 540 mM HS ion concentration. For NaCl, $NaNO_3$, and KCl the AHDs significantly increased with increasing HS ion concentration over the measured range ($p < 0.05$, two-sample F-test and T-test between neighboring AHDs). However, AHD differences were not significantly different ($p > 0.05$, two-sample F-test and T-test between neighboring AHDs) for LiCl and for the Na^+/PO_4^{3-} buffer over the measured concentration range. This was also true for NaBr in the range between 60 and 540 mM. The high scatter of the triplicates for SB with 540 mM Na^+/PO_4^{3-} buffer was most likely due to system instabilities because of the high salt concentration leading to too low density differences between the VP buoyant density (ρ_{VP}) and the GB density (ρ_{GB}).

Interestingly, AHDs for $CaCl_2$ significantly decreased with increasing concentrations over the

measured range ($p < 0.05$, two-sample F-test and T-test between neighboring AHDs). Therefore, cations as well as anions seem to be involved in the observed AHD changes, as the used Na^+ and Cl^- salts show different behavior depending on their counterion. One explanation for these observable trends could be that an increased ion concentration leads to increased ion adsorption on the VP surface which in turn leads to a larger size and density of the VPs and, accordingly, a larger AHD. However, this explanation does not fit for the Na^+/PO_4^{3-} buffer, for the NaBr buffer at higher concentrations, and for all concentrations of the $CaCl_2$ buffer. Other explanations for this phenomenon could be that different VP rigidities result in different AHDs with buffer change, the presence of ion channels in the membrane of cell-derived VPs which change their activity depending on the HS ion present that leads to changes in VP density and/or size, or the option that different GB interact differently with VPs than with the standard particles used for calibration.

The virus PSDs of A/PR_{SUS} at a concentration of 20 mM are shown in Figure 3A, B. Here, a direct HS trend was observable for cations with $Na^+ < K^+ < Li^+ < Mg^{2+}$ and Ca^{2+} as well as for the halogen anions with $Cl^- < Br^- < I^-$. (Differences between neighboring AHDs were not significant, however; $p > 0.05$, two-sample F-test and T-test; details shown in Supplement Table 2.) In addition, the aggregation behavior was similar for all cations and anions in the size range from 60 to 240 nm, except for Li^+ which showed slightly increased aggregate levels from 100 to 220 nm. Moreover, dialysis against SB including 20 mM $CaCl_2$ resulted in aggregates with an AHD of up to 560 nm shown in detail in Figure 4A.

Furthermore, the screening of the 60 mM HS ions showed no considerable aggregation in the size range from 60 to 240 nm visualized in Figure 3C ,D, except for SB with 60 mM $CaCl_2$ were again aggregates of a size of up to 560 nm were formed (also see Figure 4A). All monomeric AHDs were in a very narrow size window of 5 nm and no significant differences could be observed ($p > 0.05$, two-sample F-test and T-test between neighboring AHDs; data not shown). Furthermore, the monomeric AHDs differ more for anions (Figure 3D). This is interesting

because influenza VPs carry a negative net-charge at pH 7.4 due to their isoelectric point in the range of 5.0 to 7.0 pI [41,42], rendering it a possible coion interaction.

Results for the SB with 540 mM HS ions are shown in Figure 3E, F. All PSDs are similar compared to SB with 60 mM HS ions (Figure 3C, D), except that the monomeric AHD range was broader for the cations. Interestingly, with $Ca^{2+} < Li^{+} < K^{+} < Na^{+}$, which is the indirect or reverse HS order, AHDs increase. Differences between neighboring AHDs were small, and only for Li^{+} and Ca^{2+} a significant difference was found ($p < 0.05$, two-sample F-test and T-test; for further details see Supplement Table 3). As for other measurements, the use of Ca^{2+} buffer resulted in aggregate formation up to a size of 560 nm (Figure 4A). Overall, the latter seems to be a general trend as VPs showed no substantial aggregation in each tested HS ion buffer for 20, 60 and 540 mM except for buffers containing Ca^{2+}. This high number of different stabilizing ions indicates a high hydrophilicity [26]. Most likely, the slightly larger effects of cations on the monomeric AHDs, especially at a concentration of 20 and 540 mM, can be attributed to the negative net-charge of the VPs. This is supported by the negative net-charge of the VPs [41,42]. The PSDs for SB with 20, 60, and 540 mM $CaCl_2$ for both samples, i.e., A/PR_{SUS} and A/PR_{ADH}, are shown in Figure 4A, B. In general, the A/PR_{ADH} VPs showed to be more aggregation prone, when compared to the A/PR_{SUS} VP. Moreover, for both VPs a shift to smaller monomeric AHDs at 540 mM $CaCl_2$ when compared to 20 and 60 mM $CaCl_2$ was observable. Furthermore, the A/PR_{ADH} VPs showed different aggregate size distributions with a large number of aggregates at all screened $CaCl_2$ concentrations when compared to the A/PR_{SUS} VP. Here, A/PR_{ADH} VPs in SB with 20 mM $CaCl_2$ even showed a potential 16-mer peak at 214 nm. This indicates a low CCC for Ca^{2+}, which corresponds to the Schulze-Hardy rule with the increased counterion valence of Ca^{2+}. However, for the other tested divalent cation (Mg^{2+}) this effect was not observed. Other possible explanations for the Ca^{2+} induced VP aggregation could be the presence of residual host-cell membrane compounds , e.g. cadherins, which are involved in Ca^{2+}-dependent adhesion of mammalian cells [43], or a decreased neuroaminidase (NA)

activity, which is also known to lead to VP aggregation [11,44]. Conversely, Ca^{2+} is also known to stabilize hydrophilic colloidal systems [26].

Comparable aggregation behavior for the A/PR_{SUS} and A/PR_{ADH} samples was observed for VPs in SB and in SB with 20 mM NaCl (Figure 4C, D). For SB the monomeric AHD for both VP samples was similar but for SB with 20 mM NaCl the monomeric AHD of A/PR_{ADH} VPs was smaller compared to A/PR_{SUS} VPs (Figure 4C, D). Additionally, VPs of A/PR_{ADH} sample showed in both cases an increased number of large aggregates compared to A/PR_{SUS} VPs. In particular, this was true for the large difference in SB with 20 mM NaCl. Here, A/PR_{SUS} VPs showed practically no aggregation compared to A/PR_{ADH} VPs which formed large aggregates consisting of multimers up to tetra- and pentamers (Figure 4D). An explanation for this difference in aggregation behavior could be differences in the glycosylation of the viral membrane protein HA [44]. Previous studies showed HA glycosylation differences for influenza VPs produced in the used suspension and adherent MDCK host-cell lines [45], which could affect VP hydrophilicities and thus VP aggregation behaviors.

4 Concluding remarks

Specific ions effects regarding the PSDs of influenza A/Puerto Rico/8/1934 (A/PR, H1N1) VP produced in a suspension (A/PR_{SUS} VP) and in an adherent MDCK host cell line (A/PR_{ADH} VP) were characterized. The experimental setup used a DCS disc centrifugation method which proved to be applicable to measure the virus PSDs after dialysis to different HS buffers.

VPs derived from both cell lines showed to be aggregation prone in low salt and Ca^{2+} containing buffers. No aggregation was visible for the other screened buffers, i.e., 60 and 540 mM for all HS ions as well as 60, 180, 540, 1020, and 1500 mM for NaCl. Furthermore, an influence of HS buffers on AHD differences of the monomeric VPs was shown for the first time that partially reflected the HS trend. In addition, A/PR_{ADH} VPs showed higher aggregation in SB with 20 mM NaCl and Ca^{2+} when compared to A/PR_{SUS}.

Whether this is due to differences in cultivation media (serum-free vs. serum-containing) or depends on the cell line ($MDCK_{SUS2}$ vs. $MDCK_{ADH}$) is not clear at the moment. However, regarding the impact of VP aggregate formation on yields in DSP as well as on formulation of vaccines, any switch from adherent to suspension cells or changes in media composition should be carefully evaluated.

Special thanks go to Pavel Marichal Gallardo for the input for the statistical evaluation, to Claudia Best, Ilona Behrendt, and Yvonne Genzel for the production of the virus material from the Max Planck Institute for Dynamics of Complex Technical Systems. Additionally, we thank Louis Villain from Sartorius Stedim Biotech GmbH for providing the TFF membrane prototypes and Marc Steinmetz from CPS Instruments Inc. for information regarding the estimation of the AHDs of aggregated spheres.

This work was supported by The German Federal Ministry of Education and Research (BMBF, 0315640C).

The authors have declared no conflicts of interest.

Supporting Information

Equations used to determine GB and VP buoyant densities according to Neumann et al. [19]; Mean diameter of monomeric influenza A/PR$_{SUS}$ virus particles in standard buffer and in standard buffer with 20, 60, 180, 540, 1020 and 1500 mM NaCl (Table S1), SB with 20 mM HS ions (Table S2), and SB with 540 mM HS ions (Table S3).

5 References

[1] Hirst, G.K., Pons, M.W., Mechanism of influenza recombination: II. Virus aggregation and its effect on plaque formation by so-called noninfective virus. Virology 1973, 56, 620–631.
[2] Young, D.C., Sharp, D.G., Poliovirus aggregates and their survival in water. Appl. Environ. Microbiol. 1977, 33, 168–177.
[3] Mattle, M.J., Crouzy, B., Brennecke, M., R. Wigginton, K., et al., Impact of Virus Aggregation on Inactivation by Peracetic Acid and Implications for Other Disinfectants. Environ. Sci. Technol. 2011, 45, 7710–7717.
[4] Wallis, C., Melnick, J.L., Virus Aggregation as the Cause of the Non-neutralizable Persistent Fraction. J. Virol. 1967, 1, 478–488.
[5] Konz, J.O., Lee, A.L., Lewis, J.A., Sagar, S.L., Development of a Purification Process for Adenovirus: Controlling Virus Aggregation to Improve the Clearance of Host Cell DNA. Biotechnology Progress 2008, 21, 466–472.
[6] Floyd, R., Sharp, D.G., Viral aggregation: quantitation and kinetics of the aggregation of poliovirus and reovirus. Applied and Environmental Microbiology 1978, 35, 1079–1083.
[7] Floyd, R., Sharp, D.G., Aggregation of poliovirus and reovirus by dilution in water. Appl. Environ. Microbiol. 1977, 33, 159–167.
[8] Floyd, R., Sharp, D.G., Viral aggregation: effects of salts on the aggregation of poliovirus and reovirus at low pH. Appl. Environ. Microbiol. 1978, 35, 1084–1094.
[9] Floyd, R., Viral aggregation: mixed suspensions of poliovirus and reovirus. Appl. Environ. Microbiol. 1979, 38, 980–986.
[10] Dunlap, R.C., Brown, E.R., Barry, D.W., Determination of the viral particle content of influenza vaccines by electron microscopy. Journal of Biological Standardization 1975, 3, 281–289.
[11] Rudneva, I.A., Kovaleva, V.P., Varich, N.L., Farashyan, V.R., et al., Influenza A virus reassortants with surface glycoprotein genes of the avian parent viruses: effects of HA and NA gene combinations on virus aggregation. Archives of Virology 1993, 133, 437–450.
[12] Campbell, J.N., Epand, R.M., Russo, P.S., Structural Changes and Aggregation of Human Influenza Virus. Biomacromolecules 2004, 5, 1728–1735.
[13] Ksenofontov, A.L., Kozlovskii, V.S., Kordyukova, L.V., Radyukhin, V.A., et al., Determination of concentration and aggregate size in influenza virus preparations from true UV absorption spectra. Mol Biol 2006, 40, 152–158.
[14] Planken, K.L., Cölfen, H., Analytical ultracentrifugation of colloids. Nanoscale 2010, 2, 1849.
[15] Scott, D.J., Harding, S.E., Rowe, A.J., Analytical Ultracentrifugation: Techniques and Methods, Royal Society of Chemistry, 2005.
[16] Jr, L.B., Fitzpatrick, S., Size distribution analysis of recombinant adenovirus using disc centrifugation. J Ind Microbiol Biotech 1998, 20, 317–322.
[17] Shih, S.-J., Yagami, M., Tseng, W.-J., Lin, A., Validation of a quantitative method for detection of adenovirus aggregation. Bioprocessing Journal 2011, 9, 25–33.
[18] Deschuyteneer, M., Elouahabi, A., Plainchamp, D., Plisnier, M., et al., Molecular and structural characterization of the L1 virus-like particles that are used as vaccine antigens in CervarixTM, the AS04-adjuvanted HPV-16 and -18 cervical cancer vaccine. Human Vaccines 2010, 6, 407–419.
[19] Neumann, A., Hoyer, W., Wolff, M.W., Reichl, U., et al., New method for density determination of nanoparticles using a CPS disc centrifugeTM. Colloids and Surfaces B: Biointerfaces 2013, 104, 27–31.
[20] Anderson, W., Kozak, D., Coleman, V.A., Jämting, Å.K., et al., A comparative study of submicron particle sizing platforms: Accuracy, precision and resolution analysis of polydisperse particle size distributions. Journal of Colloid and Interface Science 2013, 405, 322–330.
[21] Kunz, W., Lo Nostro, P., Ninham, B.W., The present state of affairs with Hofmeister effects. Current Opinion in Colloid & Interface Science 2004, 9, 1–18.

[22] Zhang, Y., Cremer, P.S., Interactions between macromolecules and ions: the Hofmeister series. Current Opinion in Chemical Biology 2006, 10, 658–663.
[23] Oncsik, T., Trefalt, G., Borkovec, M., Szilagyi, I., Specific Ion Effects on Particle Aggregation Induced by Monovalent Salts within the Hofmeister Series. Langmuir 2015.
[24] Kunz, W., Specific ion effects in colloidal and biological systems. Current Opinion in Colloid & Interface Science 2010, 15, 34–39.
[25] Oncsik, T., Trefalt, G., Csendes, Z., Szilagyi, I., et al., Aggregation of Negatively Charged Colloidal Particles in the Presence of Multivalent Cations. Langmuir 2014, 30, 733–741.
[26] López-León, T., Santander-Ortega, M.J., Ortega-Vinuesa, J.L., Bastos-González, D., Hofmeister Effects in Colloidal Systems: Influence of the Surface Nature. J. Phys. Chem. C 2008, 112, 16060–16069.
[27] López-León, T., Jódar-Reyes, A.B., Ortega-Vinuesa, J.L., Bastos-González, D., Hofmeister effects on the colloidal stability of an IgG-coated polystyrene latex. Journal of Colloid and Interface Science 2005, 284, 139–148.
[28] Pavlovic, M., Huber, R., Adok-Sipiczki, M., Nardin, C., et al., Ion specific effects on the stability of layered double hydroxide colloids. Soft Matter 2016, 12, 4024–4033.
[29] Oncsik, T., Desert, A., Trefalt, G., Borkovec, M., et al., Charging and aggregation of latex particles in aqueous solutions of ionic liquids: towards an extended Hofmeister series. Phys. Chem. Chem. Phys. 2016, 18, 7511–7520.
[30] Tian, R., Yang, G., Li, H., Gao, X., et al., Activation energies of colloidal particle aggregation: towards a quantitative characterization of specific ion effects. Phys. Chem. Chem. Phys. 2014, 16, 8828–8836.
[31] Beynon, P.R., Easterby, J., Buffer Solutions, Taylor & Francis, Oxford ; New York 1996.
[32] Kalbfuss, B., Knöchlein, A., Kröber, T., Reichl, U., Monitoring influenza virus content in vaccine production: Precise assays for the quantitation of hemagglutination and neuraminidase activity. Biologicals 2008, 36, 145–161.
[33] Lohr, V., Genzel, Y., Behrendt, I., Scharfenberg, K., et al., A new MDCK suspension line cultivated in a fully defined medium in stirred-tank and wave bioreactor. Vaccine 2010, 28, 6256–6264.
[34] Kluge, S., Benndorf, D., Genzel, Y., Scharfenberg, K., et al., Monitoring changes in proteome during stepwise adaptation of a MDCK cell line from adherence to growth in suspension. Vaccine 2015.
[35] Peschel, B., Frentzel, S., Laske, T., Genzel, Y., et al., Comparison of influenza virus yields and apoptosis-induction in an adherent and a suspension MDCK cell line. Vaccine 2013, 31, 5693–5699.
[36] Casterlain, C., Genot, C., Conformational changes of bovine serum albumin upon its adsorption in dodecane-in-water emulsions as revealed by front-face steady-state fluorescence. Biochimica et Biophysica Acta (BBA) - General Subjects 1994, 1199, 59–64.
[37] Jorgensen, L., Moeller, E.H., van de Weert, M., Nielsen, H.M., et al., Preparing and evaluating delivery systems for proteins. European Journal of Pharmaceutical Sciences 2006, 29, 174–182.
[38] CPS Disc Centrifuge - Technical Note - How to measure particle density. n.d.
[39] Verdurmen, E.M., Albers, J.G., German, A.L., Polybutadiene latex particle size distribution analysis utilizing a disk centrifuge. Colloid Polym Sci 1994, 272, 57–63.
[40] Sugita, Y., Noda, T., Sagara, H., Kawaoka, Y., Ultracentrifugation deforms unfixed influenza A virions. Journal of General Virology 2011, 92, 2485–2493.
[41] Michen, B., Graule, T., Isoelectric points of viruses. Journal of Applied Microbiology 2010.
[42] Wolf, M.W., Reichl, U., Downstream processing of cell culture-derived virus particles. Expert Review of Vaccines 2011, 10, 1451–1475.

[43] Peshwa, M.V., Kyung, Y.-S., McClure, D.B., Hu, W.-S., Cultivation of mammalian cells as aggregates in bioreactors: Effect of calcium concentration of spatial distribution of viability. Biotechnology and Bioengineering 1993, 41, 179–187.
[44] Fields Virology, 4th Edition, Fourth edition, Lippincott Williams & Wilkins, New York, NY 2001.
[45] Rödig, J.V., Rapp, E., Bohne, J., Kampe, M., et al., Impact of cultivation conditions on N-glycosylation of influenza virus a hemagglutinin produced in MDCK cell culture. Biotechnology and Bioengineering 2013, 110, 1691–1703.

Figure legends

Figure 1. (A) Measurement of the time differences for differential centrifugal sedimentation of adherent cell culture-derived influenza A virus particles (A/PR_{ADH}) and standard particles to determine the virus particle density. (Note: The 105 nm particle standard shows aggregation up to tetramers. Peak identity was confirmed by separate injection of the sample and the particle standards.) (B) Size distributions of suspension cell culture-derived influenza A virus particles (A/PR_{SUS}) dialyzed against standard buffer (SB, 10 mM Tris-HCl pH 7.4) and SB with 20, 60, 180, 540, 1020, and 1500 mM NaCl.

Figure 2. Change of the apparent hydrodynamic diameter maximum with increasing salt concentrations for monomeric suspension cell culture-derived influenza A virus particles (A/PR_{SUS}) dialyzed against standard buffer (SB, 10 mM Tris-HCl pH 7.4) with 20, 60, and 540 mM Hofmeister series ion concentration. Monomeric apparent hydrodynamic diameter maxima (AHD) trends are indicated by arrows at the top for easy visualization. Results from the $MgCl_2$, the Na_2SO_4, and the NaI containing buffers are not shown because the monomeric ADHs were not measurable at 540 mM as differences between the virus particle buoyant density and the gradient buffer density were too small.

Figure 3. (A) Cations and (B) anions particle size distributions (PSD) of suspension cell culture-derived influenza A virus particles (A/PR_{SUS}) dialyzed against standard buffer (SB, 10 mM Tris-HCl pH 7.4) with 20 mM Hofmeister series (HS) ions. (C) Cations and (D) anions PSD of A/PR_{SUS} dialyzed against SB with 60 mM HS ions. (E) Cations and (F) anions PSD of A/PR_{SUS} dialyzed against SB with 540 mM HS ions. Results from $MgCl_2$, Na_2SO_4, and NaI containing buffers were not measurable due to the very low density differences between the virus particle buoyant density and the gradient buffer density.

Figure 4. (A) Size distributions of suspension cell culture-derived influenza A virus particles (A/PR_{SUS}) and (B) adherent cell culture-derived influenza A virus particles (A/PR_{ADH}) dialyzed against standard buffer (SB, 10 mM Tris-HCl pH 7.4) with 20, 60, and 540 mM $CaCl_2$. (C) Size distributions of A/PR_{SUS} and A/PR_{ADH} virus particles dialyzed against SB and (D) SB with 20 mM NaCl.

Table S1. Mean diameter of monomeric influenza A/PR_{SUS} virus particles in standard buffer and in standard buffer with 20, 60, 180, 540, 1020 and 1500 mM NaCl. AHDs increase with increasing NaCl concentrations; differences between the successive neighboring AHDs were statistically significant ($p < 0.05$) except for 540 mM and 1020 mM ($p > 0.05$).

Table S2. Mean diameters of monomeric influenza A/PR_{SUS} virus particles in standard buffer* with 20 mM Hofmeister series ions. A direct Hofmeister series trend was observable for the cations, i.e. $Na^+ < K^+ < Li^+ < Mg^{2+}$ and Ca^{2+}, and the anions, i.e. $Cl^- < Br^- < I^-$; differences between neighboring AHDs were not significant ($p > 0.05$).

Table S3. Mean diameters of monomeric influenza A/PR_{SUS} virus particles in standard buffer* with 540 mM Hofmeister series ions. The AHD order of the cations partially reflected a full indirect Hofmeister series trend: $Na^+ > K^+ > Li^+ > Ca^{2+}$. However, the differences between the neighboring AHDs were only statistically significant between Li^+ and Ca^{2+} ($p < 0.05$) and neither between Na^+ and K^+ nor K^+ and Li^+ ($p > 0.05$).

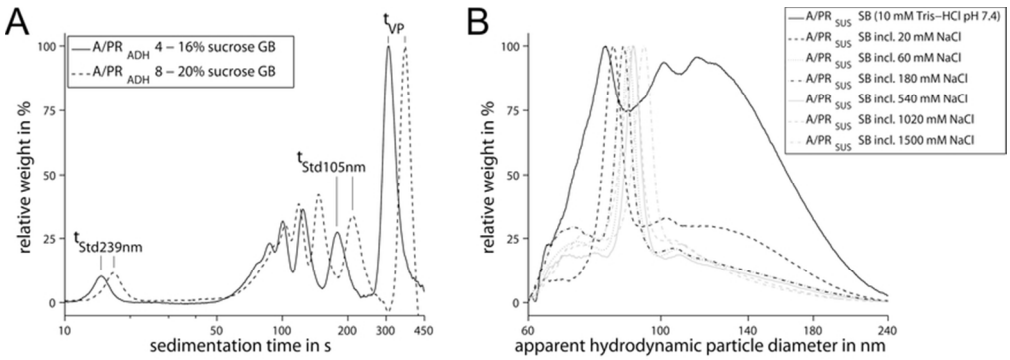

Figure 1. (A) Measurement of the time differences for differential centrifugal sedimentation of adherent cell culture-derived influenza A virus particles (A/PR_{ADH}) and standard particles to determine the virus particle density. (Note: The 105 nm particle standard shows aggregation up to tetramers. Peak identity was confirmed by separate injection of the sample and the particle standards.) (B) Size distributions of suspension cell culture-derived influenza A virus particles (A/PR_{SUS}) dialyzed against standard buffer (SB, 10 mM Tris-HCl pH 7.4) and SB with 20, 60, 180, 540, 1020, and 1500 mM NaCl.
73x25mm (300 x 300 DPI)

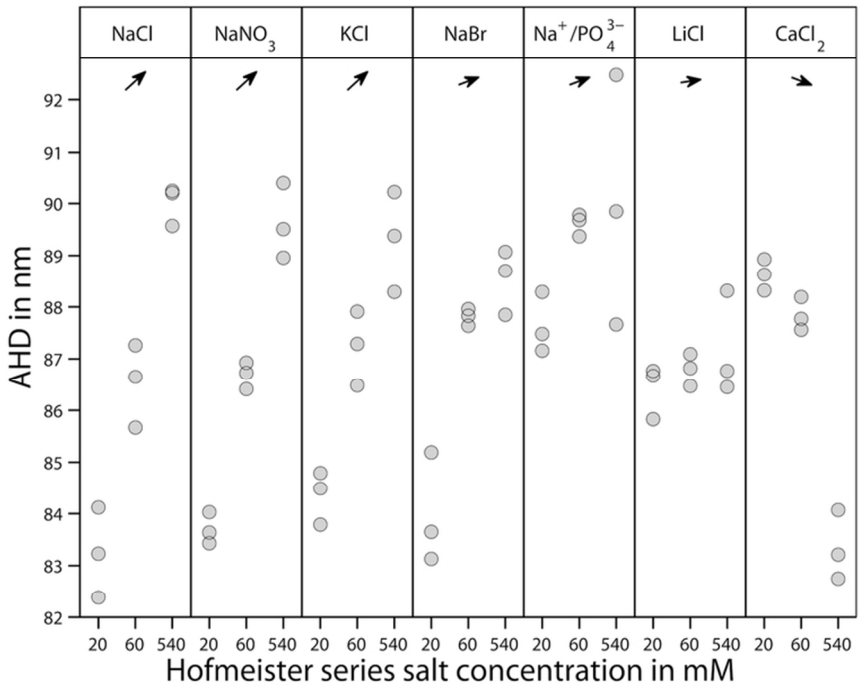

Figure 2. Change of the apparent hydrodynamic diameter maximum with increasing salt concentrations for monomeric suspension cell culture-derived influenza A virus particles (A/PR_{SUS}) dialyzed against standard buffer (SB, 10 mM Tris-HCl pH 7.4) with 20, 60, and 540 mM Hofmeister series ion concentration. Monomeric apparent hydrodynamic diameter maxima (AHD) trends are indicated by arrows at the top for easy visualization. Results from the MgCl2, the Na2SO4, and the NaI containing buffers are not shown because the monomeric ADHs were not measurable at 540 mM as differences between the virus particle buoyant density and the gradient buffer density were too small.
75x56mm (300 x 300 DPI)

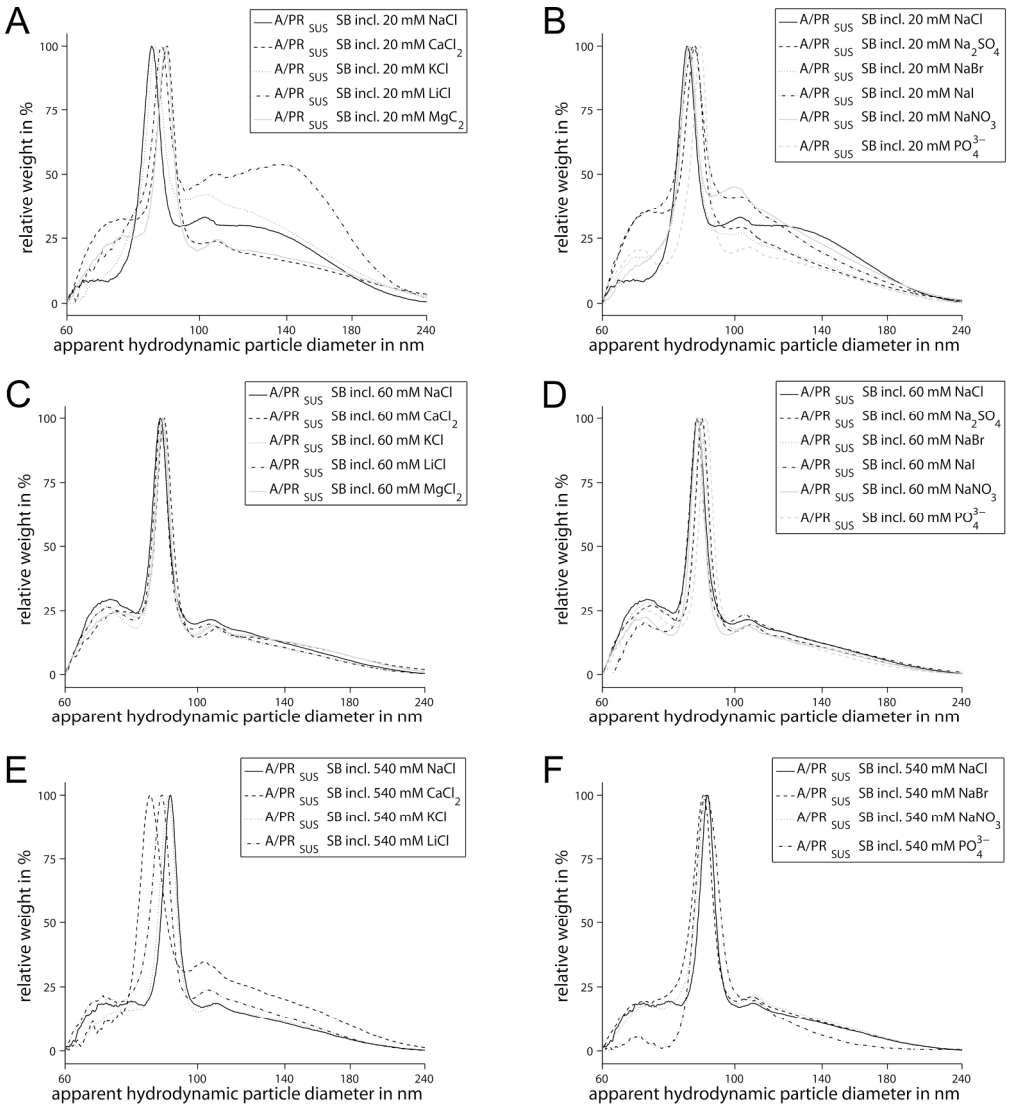

Figure 3. (A) Cations and (B) anions particle size distributions (PSD) of suspension cell culture-derived influenza A virus particles (A/PR_{SUS}) dialyzed against standard buffer (SB, 10 mM Tris-HCl pH 7.4) with 20 mM Hofmeister series (HS) ions. (C) Cations and (D) anions PSD of A/PR_{SUS} dialyzed against SB with 60 mM HS ions. (E) Cations and (F) anions PSD of A/PR_{SUS} dialyzed against SB with 540 mM HS ions. Results from $MgCl_2$, Na_2SO4, and NaI containing buffers were not measurable due to the very low density differences between the virus particle buoyant density and the gradient buffer density.
233x259mm (300 x 300 DPI)

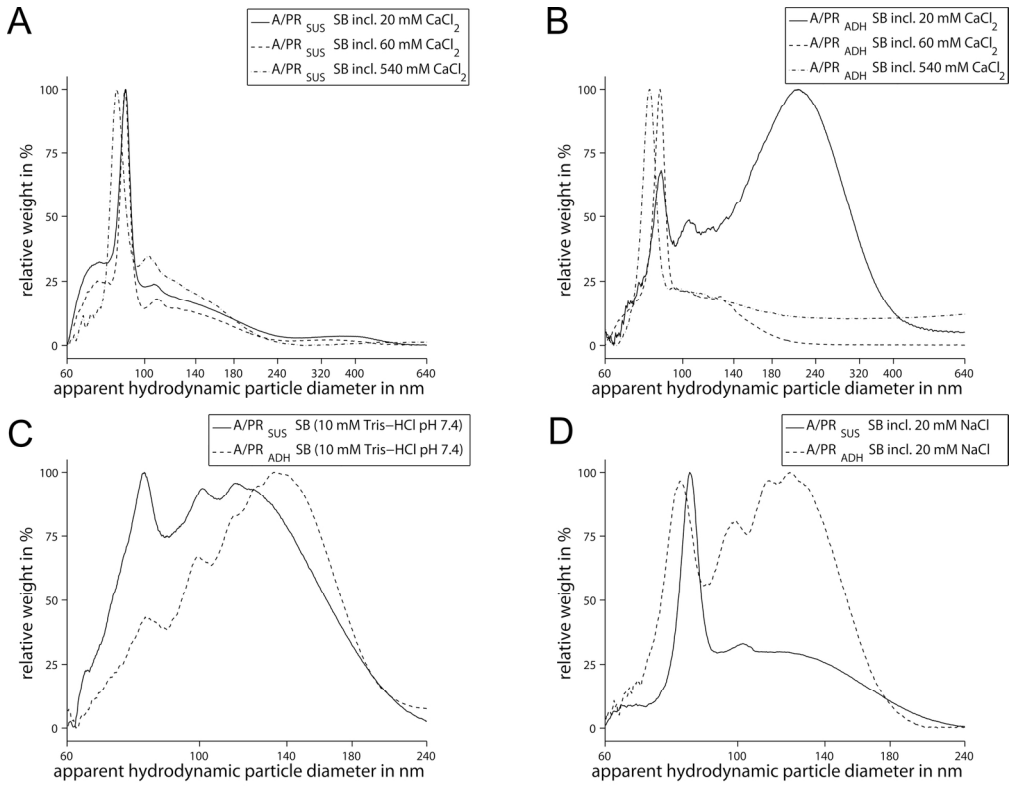

Figure 4. (A) Size distributions of suspension cell culture-derived influenza A virus particles (A/PR_{SUS}) and (B) adherent cell culture-derived influenza A virus particles (A/PR_{ADH}) dialyzed against standard buffer (SB, 10 mM Tris-HCl pH 7.4) with 20, 60, and 540 mM $CaCl_2$. (C) Size distributions of A/PR_{SUS} and A/PR_{ADH} virus particles dialyzed against SB and (D) SB with 20 mM NaCl.
163x126mm (300 x 300 DPI)

Supporting information for the article "Specific ion effects on the particle size distributions of cell culture-derived influenza A virus particles within the Hofmeister series"

Authors:
Michael M. Pieler[1,*], Anja Schenk[2], Michael W. Wolff[1,2], Udo Reichl[1,2]

[1] Max Planck Institute for Dynamics of Complex Technical Systems, Sandtorstr. 1, 39106 Magdeburg, Germany
[2] Otto von Guericke University Magdeburg, Universitätsplatz 2, 39106 Magdeburg, Germany

Corresponding Author:
*Tel.: +49 391 67 54673, E-mail: pieler@mpi-magdeburg.mpg.de

Supporting information:
Equations used to determine GB and VP buoyant densities according to Neumann et al.; Mean diameter of monomeric influenza A/PR_{SUS} virus particles in standard buffer and in standard buffer with 20, 60, 180, 540, 1020 and 1500 mM NaCl (Table S1), SB with 20 mM HS ions (Table S2), and SB with 540 mM HS ions (Table S3).

Equations used to determine GB and VP buoyant densities according to Neumann et al. [19]:

$$x_i = \rho_i;\ y_i = \frac{1}{t_i(D_i)^2};\ i = Std1\ or\ Std2 \quad (1)$$

$$\Delta y = k\Delta x + d \rightarrow k = \frac{\Delta y}{\Delta x} \rightarrow d = y_i - kx_i \quad (2)$$

$$y = 0 \rightarrow \frac{-d}{k} = \frac{-y_i + \frac{\Delta y x_i}{\Delta x}}{\frac{\Delta y}{\Delta x}} = \rho_{GB} \quad (3)$$

$$a_j = \rho_j;\ b_j = (\rho_{Std} - \rho_j)\frac{t_{Std105nm}}{t_{VP}};\ j = GB4 - 16\%\ or\ GB8 - 20\% \quad (4)$$

$$\Delta b = e\Delta a + g \rightarrow e = \frac{\Delta b}{\Delta a} \rightarrow g = b_j - ea_j \quad (5)$$

$$b = 0 \rightarrow \frac{-g}{a} = \frac{-b_j + \frac{\Delta b a_j}{\Delta a}}{\frac{\Delta b}{\Delta a}} = \rho_{VP} \quad (6)$$

Table S1. Mean diameter of monomeric influenza A/PR$_{SUS}$ virus particles in standard buffer and in standard buffer with 20, 60, 180, 540, 1020 and 1500 mM NaCl. AHDs increase with increasing NaCl concentrations; differences between the successive neighboring AHDs were statistically significant ($p < 0.05$) except for 540 mM and 1020 mM ($p > 0.05$).

Concentration of NaCl in standard buffer* in mM	AHD in nm
0	80.92 ± 0.44
20	83.24 ± 0.50
60	86.53 ± 0.46
180	88.25 ± 0.18
540	90.00 ± 0.22
1020	89.32 ± 0.89
1500	93.74 ± 0.19

* Standard buffer 10 mM Tris-HCl pH 7.4 with NaCl. AHD as mean ± standard error of the mean (n = 3).

Table S2. Mean diameters of monomeric influenza A/PR$_{SUS}$ virus particles in standard buffer* with 20 mM Hofmeister series ions. A direct Hofmeister series trend was observable for the cations, i.e. $Na^+ < K^+ < Li^+ < Mg^{2+}$ and Ca^{2+}, and the anions, i.e. $Cl^- < Br^- < I^-$; differences between neighboring AHDs were not significant ($p > 0.05$).

HS ion	AHD in nm
Na^+	83.24 ± 0.50
K^+	84.36 ± 0.30
Li^+	86.42 ± 0.30
Mg^{2+}	87.57 ± 0.71
Ca^{2+}	88.63 ± 0.18
Cl^-	83.24 ± 0.50
Br^-	83.99 ± 0.62
I^-	85.03 ± 1.09

* Standard buffer 10 mM Tris-HCl pH 7.4 with 20 mM HS ion. AHD as mean ± standard error of the mean (n = 3).

Table S3. Mean diameters of monomeric influenza A/PR$_{SUS}$ virus particles in standard buffer* with 540 mM Hofmeister series ions. The AHD order of the cations partially reflected a full indirect Hofmeister series trend: $Na^+ > K^+ > Li^+ > Ca^{2+}$. However, the differences between the neighboring AHDs were only statistically significant between Li^+ and Ca^{2+} ($p < 0.05$) and neither between Na^+ and K^+ nor K^+ and Li^+ ($p > 0.05$).

HS ion	AHD in nm
Na^+	90.00 ± 0.22
K^+	89.30 ± 0.56
Li^+	87.18 ± 0.57
Ca^{2+}	83.34 ± 0.39

* Standard buffer 10 mM Tris-HCl pH 7.4 with 540 mM HS ion. AHD as mean ± standard error of the mean (n = 3).